J. Biochem. 2009;145(4)481–491
doi:10.1093/jb/mvn185

In Vitro and *In Vivo* Interactions of Ferredoxin-NADP$^+$ Reductases in *Pseudomonas putida*

Jinki Yeom[1], Che Ok Jeon[2], Eugene L. Madsen[3] and Woojun Park[1,*]

[1]Division of Environmental Science and Ecological Engineering, Korea University, Seoul 136-075; [2]Department of Life Science, Chung-Ang University, Seoul 156-756, Korea; and [3]Department of Microbiology, Cornell University, Ithaca, NY 14853-8101, USA

Received November 26, 2008; accepted December 26, 2008; published online January 3, 2009

Ferredoxin-NADP$^+$ reductase (Fpr) is known to control NADP$^+$/NADPH pool in proteobacteria. There is only one *fpr* gene present in most proteobacteria, but *Pseudomonas putida* has two Fprs (FprA and FprB). We elucidated the functional relationships between the two types of Fpr and their electron transport partners [ferredoxin (Fd) and flavodoxin (Fld)] by cloning, expressing and preparing these proteins in various combinations and assessing their properties *in vitro* and *in vivo* using biochemical assays, the Far-western analysis, the yeast two-hybrid assay and structural molecular modelling. Both of the Fprs have a lower K_m value for NADPH than for NADH in the diaphorase assays. With NADH as electron donor, FprB also has a high specific constant (k_{cat}/K_m) in the diaphorase assay. The catalytic efficiency of FprA is higher when Fld is present as its redox partner, compared to the kinetics observed with other electron transport partners in a NADPH-dependent cytochrome *c* reduction assay. The highest specific constant (k_{cat}/K_m) of FprB was observed in the presence of FdA. FprB's K_m value and catalytic activity (k_{cat}) with NADH were significant in cytochrome *c* reduction assays. Strong kinetic interactions of Fprs with their redox partners were also demonstrated by homology modelling, the Far-western analysis and the *in vivo* yeast two-hybrid system. This study demonstrates for the first time that Fprs in *P. putida* function as diaphorase, Fd/Fld reductases and determines their preferred redox partner *in vivo* and *in vitro*.

Key words: far-western blot, homology modelling, oxidative stress, protein-protein interaction, *Pseudomonas putida* KT2440.

Abbreviations: Fpr, Ferredoxin-NADP$^+$ reductase; Fd, [2Fe-2S] Ferredoxin; 4Fd, [4Fe-4S] Ferredoxin; Fld, Flavodoxin; FdxA, [4Fe-4S] Ferredoxin of *P. Putida* similar to FdI of *A. vinelandii*; DPIP, 2,6-dichlorophenolindophenol; NBT, Nitroblue tetrazolium.

INTRODUCTION

The Ferredoxin-NADP$^+$ reductases (Fprs; EC 1.18.1.2) are ubiquitous, monomeric and reversible flavin enzymes. Fprs display a strong preference for NADPH over NADH. They have a prosthetic flavin cofactor (FAD) and catalyse the reversible electron exchange between NADPH and either ferredoxin (Fd) or flavodoxin (Fld) (*1*, *2*). In oxygenic photosynthesis, the Fd is reduced by the photosystem, then passes electrons on to NADP$^+$ via the Fpr. This reaction provides the cellular NADPH/NADP pool needed for CO_2 assimilation and other biosynthetic processes (*3*). In heterotrophic organisms, reduced ferredoxin, owing to the reverse enzymatic activity of the Fpr, can donate an electron to several Fd-dependent enzymes, such as nitrite reductase, sulfite reductase, glutamate synthase and Fd-thioredoxin reductase, allowing ferredoxin to function in a variety of systems (*4*–*7*). Furthermore, Fd is known to be involved in the assembly of iron-sulfur clusters (*7*, *8*).

Generally, Fpr interacts with [2Fe-2S] Fd in the electron transfer process, although one of the redox partners of the *Azotobacter vinelandii* Fpr is FdI which is encoded by *fdxA* gene (*9*). The FdI (hereinafter referred to as FdxA) contains two types of [4Fe-4S] cofactor: one $[3Fe\text{-}4S]^{+/0}$ and the other $[4Fe\text{-}4S]^{2+/+}$ centre (*9*, *10*). Some bacteria and algae possess a flavodoxin (Fld) which has a flavin mononucleotide (FMN) cofactor. Fld is known to be a highly acidic protein that can substitute for Fd as the electron carrier under iron-depleted conditions. Fld is also able to efficiently substitute for Fd by accepting electrons from Fpr in various metabolic processes, including photosynthesis, nitrogen fixation, biotin synthesis and nitric oxide synthesis (*11*, *12*). Recently, Carrillo's research group has shown that a bacterial Fld is able to act as a functional substitute for the chloroplast Fd, resulting in enhanced plant tolerance to iron starvation (*13*).

P. putida carries just one Fld-encoding gene, *mioC* which was found in *Escherichia coli* to be an electron carrier for biotin synthesis (*5*). The role of the *mioC* in *P. putida* has not been determined (*5*, *14*) but it is located close to genes encoding signal transduction kinases; whereas the *mioC* of *E. coli* is located close to

*To whom correspondence should be addressed: Tel: +82-2-3290-3067, Fax: +82-2-953-0737, E-mail: wpark@korea.ac.kr

the *oriC* gene which is involved in cell division and chromosome replication (*14*). Due to the number of different physiological roles for both Fd and Fld, electron exchange between Fpr and either Fd or Fld is a very important cellular process in both eukaryotic and prokaryotic cells.

The crystal structures of several Fpr proteins, from diverse organisms, have been revealed (*15*, *16*). The protein consists of two domains. The first is made up of a scaffold of six anti-parallel strands arranged in two perpendicular β-sheets, and binds to FAD. The FAD cofactor binds to the protein through hydrogen bonds, van der Waals' contacts, and stacking interaction. The second domain (C-terminal) contains an NADP(H) binding site within a core of five parallel β-strands surrounded by seven α-helices (*2*, *14*, *16*). Fd binds to a concave surface of the FAD binding region of the Fpr, to transfer electrons (*15*). The hydrophobic environment generates entropic changes, which give rise to the transfer of electrons between the electron donor and acceptor. Thus, catalytic activity is generated in the hydrophobic cleft region, near the FAD-binding site (*15*). This cleft region in Fpr interacts with both Fd and Fld, despite their structural distinctions (*17*).

Knowledge of the evolutionary relationships between bacterial and plastid-type Fprs is limited. Bacterial Fprs are smaller and have less than 20% amino acid similarity with plastid-type Fprs, although the 3D structures of these proteins are similar, and highly conserved. The catalytic activity (k_{cat}) of the plastid-type Fprs is much higher (200–500 s^{-1}) than that of the bacterial Fprs (1–2 s^{-1}) (*1*, *2*). Bacterial Fprs can be further categorized into two subclasses, based on their amino acid similarities. The key C-terminal residue in subclass I Fpr is phenylalanine, and in subclass II Fpr is tryptophan (*2*). These residues interact with the adenine moiety of the FAD cofactor. Commonly, bacteria have one *fpr* gene in their chromosome. However, some proteobacteria, including *P. putida*, possess two annotated *fpr* genes (*fprA* and *fprB*) (*18*, *19*), whose function and evolution are unclear. Previously, it was shown that bacterial subclass I and subclass II have different metabolic functions (*2*). Because the FprA and FprB have homologues with the *A. vinelandii* Fpr (an Fpr of bacterial subclass I) and the *E. coli* Fpr (bacterial subclass II), respectively, we postulate that FprA and FprB might show different catalytic activities and relationships to metabolic commitment. The *fpr* gene in *E. coli* is known to be expressed during oxidative stress defense, and its expression is regulated by the *soxRS* system (*20*, *21*). However, the organization and regulation of the *fpr* genes in *P. putida* are known to differ from those of *E. coli* system. Little is known about the function of Fpr in *P. putida*. In the *P. putida* chromosome, two [2Fe-2S] ferredoxins (FdA and FdB), three [4Fe-4S] ferredoxins (4FdA, 4FdB and FdxA) and one flavodoxin (Fld) are annotated (Fig. 1), but their functions are unknown. To elucidate the function of the Fpr and its possible redox partners in *P. putida*, all components were cloned and purified, and *in vitro* and *in vivo* interactions of each Fpr with several Fds and Flds were performed using a variety of biochemical

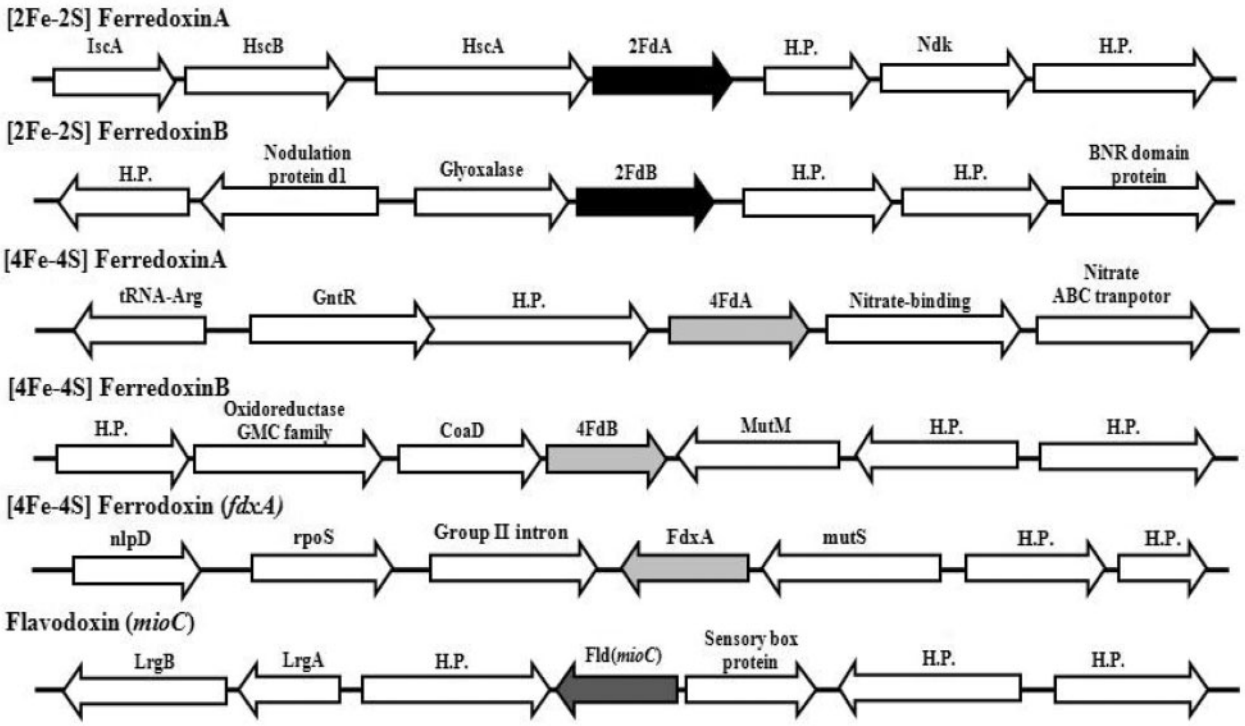

Fig. 1. **Alignment of gene cluster near ferredoxins and flavodoxin in *P. putida* KT2440.** '2Fd' indicates [2Fe-2S] Ferredoxin (black colour), '4Fd' indicates [4Fe-4S] Ferredoxin (light grey colour) and 'Fld' indicates Flavodoxin (dark grey colour). 'H.P.' indicates hypothetical protein.

assays, the yeast two-hybrid assay and homology computer modelling. Surprisingly, we found that FprA is a flavodoxin-$NADP^+$ reductase. FprB, ferredoxin-$NADP^+$ reductase, interacts efficiently with FdA.

EXPERIMENTAL PROCEDURES

Bacterial Strains, Plasmids and Growth Conditions—Bacterial strains and plasmids are described in Table S1. Antibiotics (kanamycin, 100 μg/ml and ampicillin, 50 μg/ml) were added when necessary. The open reading frame (ORF) of the *fprA* gene was amplified by PCR using FprA-OE1 and FprA-YT2 primer pairs, and the *fprB* ORF was amplified using FprB-OE1 and FprB-OE2 primer pairs. The amplified fragments, containing the *fprA* and *fprB* genes, were cloned into the *Nde*I/*Sal*I sites of pET-28a(+), yielding pET-*fprA* and pET-*fprB*. The pET-*fprA* and pET-*fprB* were transformed into *E. coli* BL21 (DE3) cells by electroporation. *E. coli* BL21 (DE3) cells were grown with moderate shaking, at a range of temperatures, in 2-YT medium supplemented with kanamycin (100 μg/ml). Cells were then grown to the mid-log phase (OD_{600} of ~0.7) at 37°C, with aeration. The cell cultures were grown at 30°C for 5–7 h after induction with 0.25 mM isopropyl thio-D-galactoside (IPTG), and then harvested. In the case of [2Fe-2S] Fds and FdxA, the ORF of *fdA* was amplified using the FDA-OE1 and YFD-A2 primer pairs, and the *fdB* ORF was amplified using FDB-OE1 and YFD-B2 and the *fdxA* ORF was amplified using FdxA-F and FdxA-R primer pairs. In the case of Fld, the ORF of *fld* (*mioC*) was amplified using the Fld-F and Fld-R. The amplified fragments, containing the *fdA*, *fdB*, *fdxA* and *fld* (*mioC)* genes, were cloned into *EcoR*I/*Xho*I sites of pET-28a(+), yielding pET-*fdA*, pET-*fdB*, pET-*fdxA* and pET-*fld*. The pET-*fdA*, pET-*fdB*, pET-*fdxA* and pET-*fld* were transformed into *E. coli* BL21 (DE3) cells by electroporation. *E. coli* BL21 (DE3) cells were grown under moderate shaking, at a range of temperatures, in 2-YT medium supplemented with kanamycin (100 μg/ml). Cells were grown to the mid-log phase (OD_{600} of ~0.7) at 30°C, with aeration. The cell cultures were grown at 25°C for 10 h after induction with 0.25 mM IPTG, and then harvested.

Protein Purification—All purification steps were performed at 4°C, using an FPLC system (AKTA FPLC, Unicorn 4.0, Amersham Bioscience). In the case of flavoproteins, Fprs and Fld, *E. coli* cell pellets were resuspended in Buffer A (50 mM Tris–Cl and 1 mM dithiothreitol, pH 7.5) and disrupted by sonication. After removal of cell debris by centrifugation at 12 000 g for 30 min, the soluble fraction was loaded onto an anion exchange column (1 ml, DEAE-cellulose, Amersham Bioscience) equilibrated with Buffer A, and the proteins were eluted with a 20 ml linear gradient of 0–1 M NaCl in Buffer A (pH 7.5). The fractions (0.5 ml each) were collected and concentrated by ultrafiltration with Centricon (2 ml YM-10, Amicon). The concentrates were applied to a Ni-NTA column (1 ml, His-trap, Amersham Bioscience) equilibrated with binding buffer (20 mM sodium phosphate, 0.5 M NaCl, 40 mM imidazole, pH 7.4), and the proteins eluted with 15 ml of elution buffer (20 mM sodium phosphate, 0.5 M NaCl, 250 mM imidazole, pH 7.4). The fractions were dialysed by ultrafiltration with Centricon (2 ml YM-10, Amicon) and stored at −80°C in 10% glycerol.

In the case of Fds and FdxA, after Ni-NTA purification according to the above methods, the fractions of Fd were applied to a gel-permeation column (Sephacryl S-200 HR 26/60, Pharmacia) and equilibrated with 50 mM Tris–Cl buffer (pH 7.5) containing 150 mM NaCl and 1 mM dithiothreitol. The proteins were eluted from the column with the same buffer at a flow rate of 30 ml h^{-1}. The sodium dodecyl sulfate polyacrylamide gel electrophoresis (SDS–PAGE) was carried out using 15% polyacrylamide gels to check the level of expression and purification. The molecular weight of the native Fpr protein was measured using size exclusion chromatography (Sephacryl S-200 HR 16/60, Amersham Bioscience). The size exclusion chromatography was calibrated with alcohol dehydrogenase (150 kDa), bovine serum albumin (67 kDa) and lysozyme (14 kDa), all known to be monomeric proteins, at a flow rate of 30 ml h^{-1}. The fractions were stored at −80°C in 10% glycerol (*22*, *23*).

Spectral Analysis of Flavoprotein—Spectral analysis was performed using an Optizen 2120 UV/VIS spectrophotometer (Mecasys, KOREA). For identification of the flavoproteins cofactors, Fpr was denatured by heating at 100°C, and the released cofactor was treated with phosphodiesterase (PDE) for 5 min. The treated sample was analysed using a fluorescence microtiter plate reader (VICTOR^3, Bio-rad). To record the extinction coefficient, the cofactors of Fpr and Fld were released by 10% SDS and calculated using $\varepsilon_{450} = 11\,300\ M^{-1}cm^{-1}$ for FAD and $\varepsilon_{446} = 12\,200\ M^{-1}cm^{-1}$ for FMN (*24*).

Homology Modelling of the Protein Complex—The interaction of Fpr with either Fd or Fld was confirmed using homology modelling with the structurally known Fprs, Fd and Fld (*25*). Homology models of Fprs and Fd or Fld were generated using the SWISS-MODEL (http://swissmodel.expasy.org) and the Protein Homology/analogY Recognition Engine (PHYRE) (Imperial College, London, version 0.2) homology modelling sites. The FprA model utilized the Fpr of *A. vinelandii*, due to its high degree of similarity with that of *P. putida*, and the FprB model utilized the *E. coli* Fpr as template models. The iron-sulfur cluster proteins and bacterial Fld formed the templates for the Fd and Fld models. PDB files were generated using the Deep View/Swiss PDB-viewer (version 3.7) and PyMOL (version 1.0) (*26*). Interaction between Fpr and substrate predicted by the ClusPro (version 2.0) (http://cluspro.bu.edu), which is the Fast Fourier Transform (FFT) based docking program (*27*, *28*) and docking model was made by PyMOL. (version 1.0).

Enzyme Kinetics for Analysis of Catalytic Activity—All chemicals using enzyme kinetics were purchased from Sigma. Enzyme kinetics was monitored using an Optizen 2120 UV/VIS spectrophotometer (Mecasys, KOREA) at 25°C under aerobic conditions, except for the ferric and flavin reductase assays. The diaphorase assay was recorded at 600 nm using 2,6-dichlorophenol-indophenol (DPIP) as the terminal electron acceptor and at 420 mm using $K_3Fe(CN)_6$ (ferricyanide) as the terminal electron acceptor in Tris–Cl buffer (100 mM; pH 8.2). In the diaphorase assay, NADPH or NADH was used as the

electron donor by using various concentrations (2, 5, 10, 20 and 200 μM). The cytochrome *c* assay used cytochrome *c* as the terminal electron acceptor and monitored at 550 nm in Tris–Cl buffer (100 mM; pH 8.2). The cytochrome *c* assay was performed in the presence of saturated concentrations of each component (NADPH, 0.25 mM; NADH, 0.25 mM and cytochrome *c*, 50 μM). Steady-state kinetic parameters for each cytochrome *c* assay were determined by using various concentrations (5, 10, 20, 50, 100 and 200 μM) of Fd, FdxA or Fld as an electron acceptor. Except where stated otherwise, the concentration of NADPH was maintained using 2.4 mM glucose-6-phosphate and 1.45 U glucose-6-phosphate dehydrogenase (*22*, *29*).

Far-Western Analysis—Hyper-immune rabbit antisera were raised against FprA and FprB. Briefly, His-FprA and His-FprB were expressed in *E. coli* and purified on anion exchange column (1 ml, DEAE-cellulose, Amersham Bioscience) and Ni-NTA column (1 ml, His-trap, Amersham Bioscience) using FPLC system. Immunoglobulin G (IgG) molecules were precipitated from the hyper-immune antisera with 50% saturated ammonium sulfate solution, resuspended in cold phosphate-buffered saline (PBS) and dialysed into PBS.

Far-western analysis of the interaction between Fprs and their electron partner proteins used standard procedures (*30*). The purified FdA, Fld and FdxA were loaded 5 μg and purified FprA and FprB were also loaded 10 μg at control experiment in the 12% native PAGE. Proteins were transferred to a PVDF membrane for overnight at 4°C. Proteins on the PVDF membrane were blocked with 5% non-fat milk solution (5% non-fat milk, 1X PBST). The blocked membrane was incubated for 1 h at room temperature with purified Fpr protein in 3% non-fat milk solution (3% non-fat milk, 1X PBST, 1% BSA, 0.2 mM NADPH). After three times washing for 10 min with 1× PBST buffer, membrane was probed for 1 h at room temperature with polyclonal anti-FprA/B antibody in 3% non-fat milk solution, washed as described above, incubated with peroxidase conjugated goat anti-rabbit Immunoglobulin G (Sigma, St Louis, MO) in 1× PBST, washed three times with 1× PBST and signal was detected using a Western Lighting Chemiluminescence Reagent Plus (PerkinElmer, USA). The band of image is analysed by ProXPRESS 2D (Perkin Elmer, USA) and Total Lab 2.0 Software (Nonlinear Dynamics, BioSystematica, UK).

Protein–Protein Interactions In Vivo—In order to monitor the interaction between Fpr and Fd *in vivo*, the yeast two-hybrid system employed, and the pSH18-34 vector was used as the reporter. The pEG202 and pJG4-5Vo vectors were used as the bait and trap, respectively. The open reading frames of the *fprA*, *fprB*, *fdA* and *fdB* genes were amplified by PCR. The amplified fragments were cloned into the *EcoR*I or *Xho*I sites of pEG202 and pJG4-5Vo, yielding pEG202-*fdA*, pEG202-*fdB*, pJG4-5Vo-*fprA* and pJG4-5Vo-*fprB*. The vectors were transformed into by *E. coli* by electroporation, and into EGY48 (pSH18-34) using heat shock methods. The β-galactosidase assay was carried out using standard procedures. The outcome was assessed by measuring the colour change using β-D-galactopyranoside (ONPG) as a substrate, with the results in Miller units. The gal promoter in the reporter vector was induced with galactose and raffinose in uracil-, tryptophan- or histidine-dropout liquid media. In the leucine-depleted dropout media, growth experiments were carried out according to previously-reported procedures (*31*).

RESULTS AND DISCUSSION

Molecular and Spectral Properties of Fprs, Ferredoxins and Flavodoxins—We found that the purified FprA and FprB proteins migrated at ~27 kDa using denaturing SDS-PAGE (data not shown). The bacterial Fpr has been shown to be a soluble monomeric protein, except in some cyanobacteria (*32*). Previously, we have shown that FprB was known as soluble monomeric protein (*19*). Consistent with these observations, FprA in *P. putida*, was also found to be monomer, as determined by fast protein liquid chromatography (FPLC) (Fig. S1A). Fpr is a flavin protein and requires a FAD cofactor (*29*). The flavins have a bright yellow colour (450 nm) and fluoresce with emission maximum at 524 nm (*29*). Both FprA and FprB exhibited the expected bright yellow colour during purification. The typical flavoprotein has absorbance peaks in the regions of 380 nm and 450 nm and shoulders at 420 nm and 470 nm (*22*, *29*). Scanning analysis using UV-visible spectroscopy of FprA and FprB suggested that both Fprs were typical flavoproteins (data not shown). FprA had absorbance peaks at 380 nm and 452 nm and an A_{280}/A_{452} value of 11.79 ± 1.92. FprB had absorbance peaks in the regions of 380 nm and 457 nm and an A_{280}/A_{457} value of 6.35 ± 0.72. The extinction coefficient of FAD is $11\,300\ M^{-1}\,cm^{-1}$, and the calculated extinction coefficient of the FprA and FprB cofactors were $11\,216 \pm 118\ M^{-1}\,cm^{-1}$ and $11\,089 \pm 298\ M^{-1}\,cm^{-1}$, respectively (Tables S2A and B). Phosphodiesterase (PDE), which breaks down FAD into FMN, was used to confirm the presence of the FAD cofactor. Both Fprs were boiled at 100°C to release the cofactor. If FAD was the cofactor for both FprA and FprB, the fluorescence would be expected to increase 10-fold after treatment with PDE, because of the difference in fluorescence between FAD and FMN. Indeed, the fluorescence of the Fpr cofactor increased by ~10-fold following PDE treatment (Table S2D), suggesting that both Fprs have non-covalently bound FAD as their prosthetic group.

Ferredoxins are known to be monomeric proteins, with the exception of some regulatory Fds (*32*). Both FdA and FdB in *P. putida* were confirmed to be ~17 kDa monomeric proteins (Fig. S1B and C). The spectral properties of Fd exhibited characteristic absorbance peaks at 342 nm, 418 nm and 458 nm, indicating that Fd has one [2Fe-2S] cofactor (data not shown) (*22*, *29*). In the case of FdxA, FdxA was found to be monomer (~15 kDa), as determined by FPLC (Fig. S1D) and the absorption spectrum exhibited characteristic peak at 425 nm, indicating FdxA has [4Fe-4S] cofactor (data not shown) (*9*).

Fld is known to have FMN as a cofactor (*5*). The Fld in *P. putida* was 15 kDa in size, as determined by SDS-PAGE, and is monomeric, as shown by FPLC (Fig. S1E). Purified Fld also had characteristics typical of flavin

Table 1. **Kinetic parameters of electron transfer by FprA and FprB to a variety of electron acceptors, as determined by the diaphorase assay.**

Electron acceptor	Electron donor	k_{cat}^{Fpr} (s^{-1})	$K_m^{NAD(P)H}$ (μM)	$k_{cat}^{Fpr}/K_m^{NAD(P)H}$ ($s^{-1}\,\mu M^{-1}$)
DPIP	NADPH			
	FprA	4.77 ± 0.17	4.79 ± 0.08	1.03 ± 0.02
	FprB	4.51 ± 0.06	3.97 ± 0.04	1.14 ± 0.08
	NADH			
	FprA	3.03 ± 0.23	63.22 ± 0.64	0.09 ± 0.01
	FprB	4.59 ± 0.23	7.17 ± 0.37	0.68 ± 0.02
Ferricyanide	NADPH			
	FprA	5.99 ± 0.11	2.45 ± 0.15	3.23 ± 0.06
	FprB	3.82 ± 0.03	3.26 ± 0.35	1.13 ± 0.04
	NADH			
	FprA	1.16 ± 0.03	10.63 ± 1.61	0.11 ± 0.03
	FprB	3.09 ± 0.07	4.64 ± 0.19	0.86 ± 0.04

[a]The experiment was repeated five times. The average and standard deviation are shown here.

proteins, with absorbance peaks at 380 nm and 452 nm and an A_{280}/A_{452} value of 12.3 ± 0.38 (Table S2C). The typical extinction coefficient of FMN is $12\,200\,M^{-1}\,cm^{-1}$, and the calculated extinction coefficient of the Fld cofactor was $12\,754 \pm 784\,M^{-1}\,cm^{-1}$. Using PDE as mentioned above, the cofactor of Fld was found to be FMN (Tables S2C and D).

The Diaphorase Activity of FprA and FprB—Fprs are known to have NADPH-dependent diaphorase activity; in this reaction, electrons are transferred from NADPH to various terminal electron acceptors such as 2,6-dichlorophenol-indophenol (DPIP) and ferricyanide (*22*, *29*). We completed eight diaphorase assays that varied key electron donor/acceptor parameters (Table 1). FprA had the highest catalytic efficiency ($k_{cat}/K_m = 3.23 \pm 0.06\,s^{-1}\mu M^{-1}$) in the presence of ferricyanide (Table 1). As shown in other reports, both Fprs prefer NADPH over NADH as an electron donor (*1*, *2*). The K_m value of both Fprs is much lower for NADPH, compared to the values obtained with NADH. It is generally agreed that the K_m value is the most important parameter in the analysis of diaphorase activity (*22*, *29*). However, we argue that both the K_m value and the catalytic efficiency of FprB with NADH are significant. The NADH-dependent electron transfer rate of the FprB was eight times higher than that of the FprA (Table 1).

In the NAD(P)H-dependent diaphorase assay, using NADPH as an electron donor and ferricyanide as an electron acceptor, the $K_m^{NAD(P)H}$ and k_{cat}^{Fpr} values of the *P. putida* Fprs were lower than the reported values for other organisms, except for *Mycobacterium tuberculosis* (Table S3). When DPIP was used as an electron acceptor, the $K_m^{NAD(P)H}$ and k_{cat}^{Fpr} values of the Fprs in *P. putida* were still lower than other organisms, except for *M. tuberculosis* (Table S3). Although the experimental conditions differed amongst the reported diaphorase assays, the conclusion to be drawn here is that the *P. putida* Fprs have a lower $K_m^{NAD(P)H}$, and lower catalytic activity (k_{cat}^{Fpr}) than the Fprs of other organisms. With the exception of *M. tuberculosis* (Table S3), diaphorase assays using NADH as the electron donor have not been reported before. Our result indicated that the FprB of *P. putida* using NADH has a very high catalytic efficiency (Table 1). *In vivo*, diaphorase activity was confirmed by the NBT assay using crude extract of wild type, *fprA* and *fprB* mutants. Results indicated that none of the treatments were significantly different from the background NBT level (data not shown). This result may be related to the fact that there are many other enzymes that function as a diaphorase (*2*).

Homology Modelling of Fprs With their Redox Partners—Based on the Fpr complex in maize leaves (*15*), the gap between flavin of Fpr and the iron-sulfur centre of Fd is about 6.0 Å. Our docking-model predictions about various Fpr-Fd complexes in *P. putida* showed the distances between the FAD and iron-sulfur cofactors to be within with 10 Å (*33*). In the case of various Fpr-substrate complexes, distance between the FAD and iron-sulfur cofactor appears to be within 10 Å (*33*). Therefore, in the Fpr-substrate complexes of *P. putida* KT2440, docking models having this distance range is considered to be plausible. Possible Fpr-substrate combinations are only shown in Fig. 2. This interaction computer modelling using the ClusPro (version 2.0) (http://cluspro.bu.edu), which is the Fast Fourier Transform (FFT)-based docking program, is found to be very informative (*27*, *28*).

In the case of FprA, the phenylalanine residue (yellow colour in Fig. 2A and B) is adjacent to the FAD cofactor. Phenylalanine has been shown to be important for proper functioning of bacterial subclass I Fpr (*2*). In modelling the complex between FprA and Fld, cofactors of these protein molecules were found to be separated by 9.79 Å (Fig. 2A). This means that the two molecules have the potential to interact and may be able to exchange electrons via cofactors. FprA also has many basic residues (Arg48, Arg52, Lys94, Lys95 and Arg245) near Fld docking location (black colour in Fig. 2A). Fld, which is more acidic than Fd, may be stabilized by basicity of Arg and Lys residues during their interaction. Homology modelling done with FprA and FdxA suggested that cofactor of FprA was separated by 8.68 Å from iron-sulfur centre of FdxA (Fig. 2B), indicating that FprA has the potential to interact with FdxA. It has been already reported that the Fpr and FdxA of *A. vinelandii* can form complex (*9*). FprA and FdxA of *P. putida* have 83.7 and 85.8% amino acid similarities with the Fpr and FdxA of *A. vinelandii*, respectively.

The tryptophan residue (yellow colour in Fig. 2C) of FprB is adjacent to the FAD cofactor. The tryptophan residue is known to be an important residue for proper functioning of Fprs (*1*, *2*). When FprB interacts with FdA, the cofactor of FprB can approach the cofactor of FdA within 5.93 Å which is the closest approach for docking of all the complexes modelled (Fig. 2C). Thus, electron transfer between FprB and FdA should be facile. The complex between FprB and FdA also emerges from this modelling exercise as the one that is the best for transferring electrons from FprB to FdA. In the case of interaction between FprB and Fld, these cofactors can interact, but FprB has fewer basic residues (Arg107, Lys246 and Arg247) in its active site compared to FprA (Fig. 2D). Therefore, the complex between FprB and Fld

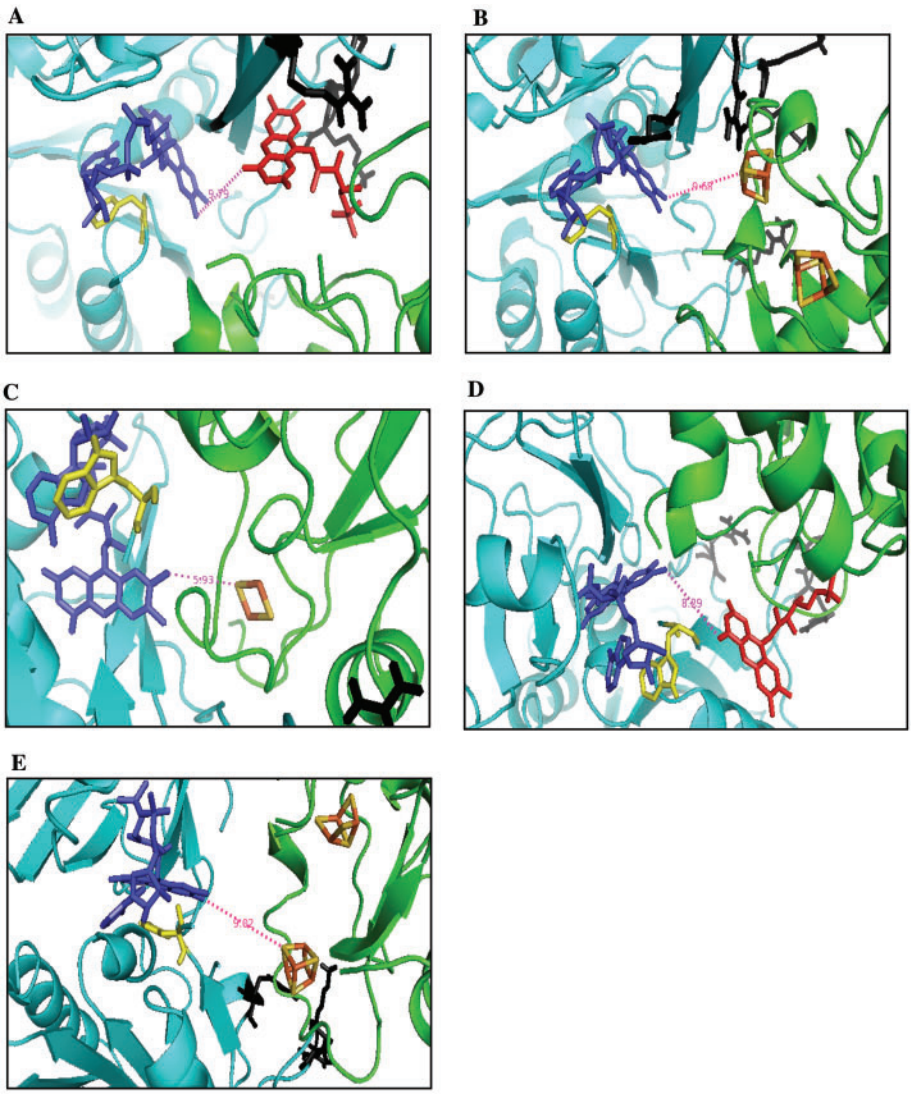

Fig. 2. **Homology protein model of the Fpr complexes.** Homology models show distance for to the active site inside within 10 Å. The colours are shown FAD in blue, FMN in red and iron–sulfur centres in brown, and basic residues near the interaction region in black, colours. Models are shown in cyan, which is Fpr in cyan, and green, which are substrates in green, respectively. (A) The complex of FprA and Fld is displayed with the active site. The phenylalanine residue near active site is shown in yellow colour. (B) The complex of FprA and FdxA is displayed. (C) The complex of FprB and FdA is displayed with the active site, and tryptophan residue is shown in yellow. The complexes of (D) FprB and Fld and (E) FprB and FdxA are displayed.

may have relatively low stability, consistent with this complex's low catalytic efficiency compared to that of FprA and Fld (Table 2). On the basis of 9.02 Å cofactor distance between FprB and FdxA in the homology modelling, it is possible to predict that FprB may be able to transfer electron to FdxA (Fig. 2E). For [2Fe-2S] FdB and [4Fe-4S] Fds, because the relatively large separation between cofactors of these proteins, these Fprs are unlikely to interact with [2Fe-2S] FdB and [4Fe-4S] Fds (data not shown).

In vitro *Interactions Between Fprs and their Redox Partners*—The kinetic properties of two Fprs with their redox partners were examined using a cytochrome *c* reduction assay (*22*, *29*). FprA had a very poor catalytic efficiency (k_{cat}^{FprA}/K_m^{Fd}) when paired with either FdA or FdB. The K_m^{FdB} values of both Fprs with FdB were high, giving rise to low catalytic efficiency (Table 2). Consistent with the homology modelling, the kinetic data strongly suggested that FdB is not a physiological redox partner of both Fprs. An Fd-dependent NAD(P)H cytochrome *c* reductase assay showed that FprB strongly preferred FdA, producing a high catalytic activity ($k_{cat} = 29.0 \pm 0.94\,s^{-1}$). The k_{cat}^{FprB} value of FprB was 10-fold higher than that of the FprA. Thus, the catalytic efficiency parameter (k_{cat}^{FprB}/K_m^{Fd}) of FprB was higher than FprA values (Table 2), indicating that FprB is likely to be an electron transfer partner with FdA. An Fd-dependent NAD(P)H cytochrome *c* reduction assay using FdA indicated that the k_m^{FdA} and k_{cat}^{FprB} values of the *P. putida* FprB were similar to those observed in *E. coli*, lower than those of other organisms (Table S3), and higher than those of *M. tuberculosis* (Table S3).

Table 2. **Kinetic parameters of electron transfer by FprA and FprB to a variety of electron acceptors, as determined by the cytochrome *c* assay.**

Electron acceptor	Electron donor	k_{cat}^{Fpr} (s^{-1})	$K_m^{Fd/Fld}$ (μM)	$k_{cat}^{Fpr}/K_m^{Fd/Fld}$ ($s^{-1}\,\mu M^{-1}$)
FdA	NADPH			
	FprA	2.61 ± 0.63	1.91 ± 0.04	1.37 ± 0.04
	FprB	28.96 ± 0.94	2.63 ± 0.26	11.02 ± 0.34
	NADH			
	FprA	2.16 ± 0.04	23.63 ± 1.61	0.09 ± 0.02
	FprB	18.88 ± 0.43	2.98 ± 0.10	6.73 ± 0.23
FdB	NADPH			
	FprA	3.18 ± 0.31	6.15 ± 0.11	0.53 ± 0.01
	FprB	5.40 ± 0.22	6.86 ± 0.14	0.77 ± 0.02
	NADH			
	FprA	1.52 ± 0.05	9.43 ± 0.21	0.17 ± 0.04
	FprB	4.33 ± 0.16	8.02 ± 0.02	0.54 ± 0.02
Fld	NADPH			
	FprA	9.22 ± 0.46	0.83 ± 0.02	11.51 ± 0.27
	FprB	6.39 ± 0.14	1.81 ± 0.04	3.72 ± 0.16
	NADH			
	FprA	1.52 ± 0.04	11.63 ± 0.31	0.13 ± 0.04
	FprB	15.30 ± 0.36	8.22 ± 0.07	1.86 ± 0.02
FdxA	NADPH			
	FprA	5.81 ± 0.01	1.91 ± 0.06	3.05 ± 0.09
	FprB	5.10 ± 0.05	1.11 ± 0.03	4.59 ± 0.32
	NADH			
	FprA	0.62 ± 0.02	9.33 ± 0.21	0.07 ± 0.02
	FprB	5.20 ± 0.23	1.12 ± 0.04	4.63 ± 0.02

[a]The experiment was repeated five times. The average and standard deviation are shown here.

Commonly, cytochrome *c* reduction assays using Fld as an electron acceptor produce much lower catalytic activities than do assays using Fd (Table S3). When Fld was used as an electron acceptor in the cytochrome *c* reduction assay, it interacted strongly with FprA, producing a very low K_m^{Fld} value. The FprA had a high catalytic efficiency (k_{cat}^{FprA}/K_m^{Fld}) when paired with Fld, indicating that Fld was the preferred redox partner of FprA (Table 2). FprA and FprB have low K_m^{FdrA} values with FdxA in the cytochrome *c* reduction assay, however, lower catalytic activities (k_{cat}^{Fpr}) were observed compared to previous combinations (FprA/Fld or FprB/FdxA). These kinetic data suggested that FdxA is not the most preferred redox partner of both Fprs, but it may have potential of redox reaction with both Fprs. (Table 2).

To confirm *in vitro* interaction of Fprs with their redox partners, the Far-western analysis was performed using purified FdA, Fld, FdxA and Fprs (Fig. 3). The 12% native PAGE is loaded with 5 μg of each FdA, FdxA and Fld in each lane, and 10 μg of FprA and FprB was used as controls (Fig. 3A). When FprA was used as a probe protein, the lane containing Fld showed very strong band intensity (~6-fold), compared with others (Fig. 3B and D). For the Far-western blot data using FprB as a probe protein, the FdA and Fld lanes showed very strong band intensity (~9-fold, Fig. 3C and D). However, the FdA lane appears to be the strongest intensity. Consistent with the previous biochemical data, Fld and FdA are the preferred redox partners for FprA and FprB, respectively. As seen in previous kinetic data (Table 2), the Far-western blot data suggested that FdxA may interact with both Fprs, but its interaction may not be stronger. In conclusion, homology modelling, the kinetic and the Far-western analysis data presented here, reinforce the hypothesis that Fld is the preferred redox partner of FprA, and that FdA is able to interact productively with FprB.

In vivo *Interactions Between Fprs and their Substrates*—The yeast two-hybrid system was used to examine interactions between the Fprs and the Fds *in vivo*. Previous studies of bacterial putidaredoxin, [a type of [2Fe-2S] ferredoxin capable of being formed in yeast], suggested that the bacterial [2Fe-2S] ferredoxin may be matured in yeasts (*34*). We thus tested interaction with Fprs *in vivo* using only [2Fe-2S] type ferredoxins in *P. putida*. To test the applicability of the yeast two-hybrid assay for our experimental goals, we conducted control runs using empty vectors. In these, the yeast strain incorporating FdA in the bait vector produced very high basal levels compared with other strains (Fig. S2). However, these could be ignored because the interaction between FprB and FdA proceeded at a much higher level (~10-fold higher than that of pEG202-FdA control strain) (Fig. 4A and B). Serial dilutions of each strain were made in leucine depletion-dropout medium under galactose/raffinose conditions. As before, the strain incorporating FprB in the trap vector, with the FdA in the bait vector, survived under galactose/raffinose conditions and no other strains grew in the glucose medium, except for the strain incorporating FdA in the bait vector, which exhibited basal levels of growth. Consistent with the *in vitro* data above (Table 2), FdB did not appear to interact with Fpr in the yeast two-hybrid system, and the complex of FdA and FprB interacted more strongly than any other complex examined (Fig. 4A and B).

To confirm the yeast two-hybrid data, Fpr and Fd were also cloned into the bait and trap vectors, respectively. When FprB was incorporated into the bait vector and FdA the trap vector, FprB also interacted strongly with FdA (data not shown). The yeast strain containing FprB and FdA shows the most efficient survival under auxotropic conditions. Consistent with the kinetic data, the *in vivo* interaction study using the yeast two-hybrid system confirmed that FprB has a more specific binding activity with FdA.

Previously, we have demonstrated that the expression of the *fprA* gene is induced by oxidative stress and is regulated by the *finR* gene product (*18*, *19*). However, the *fprB* gene is not induced by oxidative stress, but is rather up-regulated by salt stress (*19*). Consistently, Western blot analysis showed that FprA was induced by a variety of oxidative stress reagents, and FprB was not (data not shown). We also measured the expression levels of *fdA*, *fld* and *fdxA* genes under various stress conditions and found that these genes are not inducible in any condition (data not shown). This observation is probably due to the fact that functions of Fds, and Flds are modulated by binding of cofactor, not by increment of their cellular amount, thus their mRNA levels are not

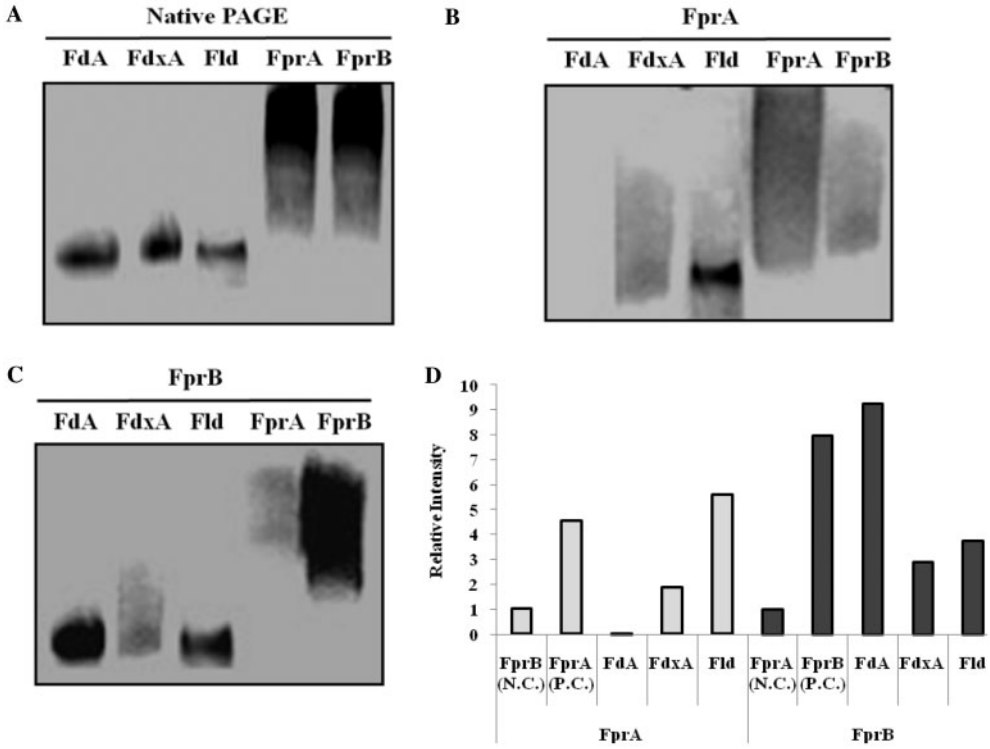

Fig. 3. **Far-western analysis of interaction between Fprs and their partners.** Five micrograms of purified FdA, Fld and FdxA are loaded and 10 μg of purified FprA and FprB are loaded as controls. Gel electrophoresis were performed using 12% native PAGE. Loading efficiency was confirmed by Coomasiae Blue R-250-staining (A). The Far-western analysis is performed by FprA probe (B) and FprB probe (C). Quantification of band intensities was measured using Total Lab 2.0 Software (Nonlinear Dynamics, BioSystematica, UK). 'N.C.' and 'P.C.' indicated negative control and positive control, respectively (D).

changed by various stress conditions (*4*, *14*). Although relative concentrations of Fpr and its substrates remain unclear, we hypothesized, based on our observation above that FprA is the preferred physiological redox partner of Fld and FprB is the preferred physiological redox partner of FdA.

FprA from *P. putida* (NP_743795.1) has an 83.7% amino acid similarity to the Fpr of *A. vinelandii* (ZP_00417949), and FprB from *P. putida* (NP_746755) has a 36.7% amino acid similarity to the Fpr of *E. coli* (NP_418359.1). In *P. putida*, FprB has 35.1% amino acid similarity with FprA. However, the two *fpr* genes of *P. putida* and *A. vinelandii* have not been characterized. All bacterial Fprs contain an NADP(H) binding domain, and use NADPH rather than NADH in their catalytic reactions (*1*, *2*, *35*). Although FprB can use NADH as electron donor, the two Fprs prefer NADPH over NADH in the diaphorase assay. Although binding of NADPH is not the rate-limiting step in this reaction (*1*, *2*), the preference for NADPH over NADH is still very important, because the balance of the NADP/NADPH pool influences the cellular electron transfer chain. The levels of $NADP^+$/NADPH in bacterial cells require maintenance by certain enzymes because NADPH is required as an electron donor in various metabolic pathways. NADPH is used by the Fprs as an electron donor and becomes $NADP^+$, and the *zwf* gene, which encodes glucose-6-phosphate dehydrogenase, is then induced, under such conditions of oxidative stress. The glucose-6-phosphate dehydrogenase reaction is reversible and from $NADP^+$ gives rise to NADPH. In this sense, the preference of NADPH for Fpr is likely to be important in maintaining the balance of NADP/NAPDH (*36*).

The interaction we found between FprA (bacterial subclass I) and Fld is surprising because the first Fpr found to function as a Fld reductase was *E. coli* Fpr, which belongs to bacterial subclass II. *P. putida* carries just one Fld-encoding gene, annotated as a *mioC*. The function of the *mioC* gene in *E. coli* was found to be an electron carrier for biotin synthesis, whereas that of the *mioC* in *P. putida* has not been determined (*5*, *14*). Our results indicated that Fld interacts strongly with FprA, having a much higher catalytic efficiency ($k_{cat}/K_m = 11.51\,s^{-1}\mu M^{-1}$) than the *E. coli* Fpr ($k_{cat}/K_m = 0.7\,s^{-1}\mu M^{-1}$; Table 2) (*1*). FprB interacts with FdA and has high catalytic activity. The FdA gene is located within the *isc-hsc* gene cluster, which is related to the iron-sulfur centre assembly (*37*). Therefore, when bacterial cells are placed under stress, FprB can transfer electrons for FdA, and reduced FdA can assist in iron-sulfur centre recovery. As such, the *isc-hsc* gene cluster seems to be involved with the iron-sulfur assembly of FdA, under iron-sulfur-depleted conditions. Thus, we propose that FprB and FdA are involved in the system for iron-sulfur centre assembly and repair under various conditions.

Most proteobacteria have just one Fpr, but *A. vinelandii* and *Pseudomonas* species have two

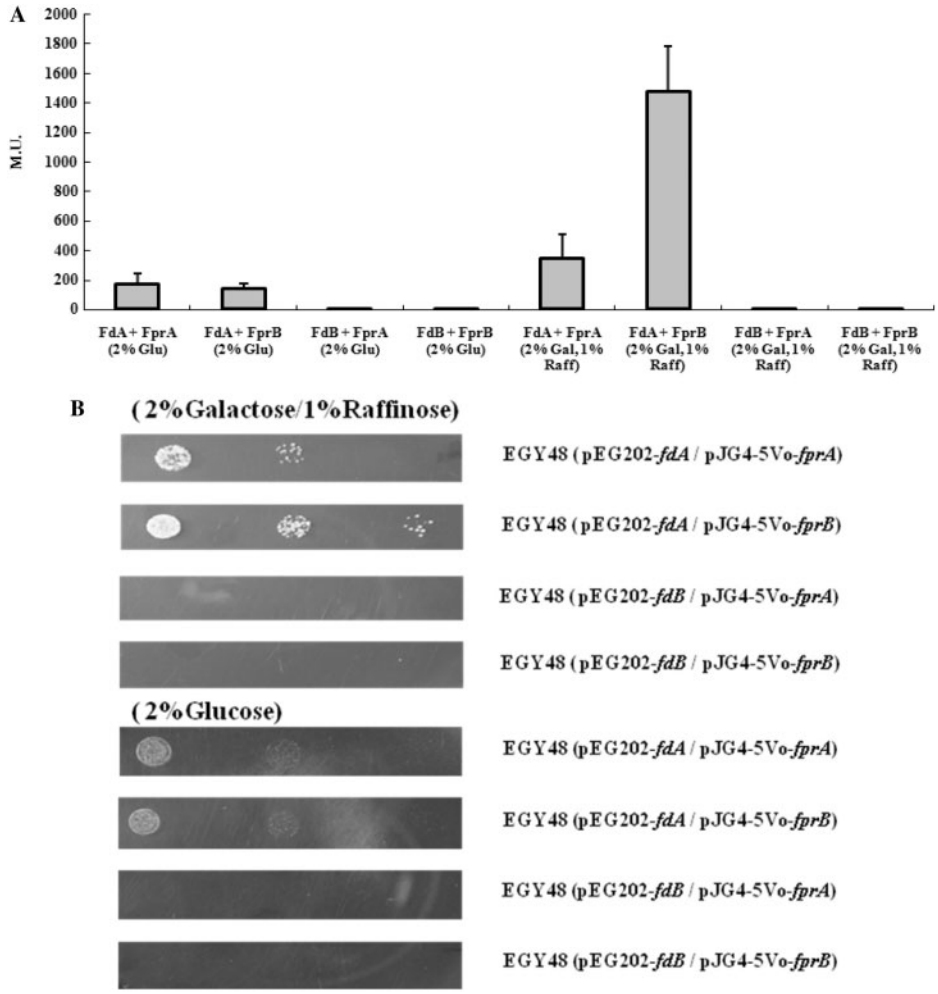

Fig. 4. **Confirmation of interaction between Fprs and Fds using the yeast two hybrid system.** The interaction between Fd in the bait vector and Fpr in the trap vector was confirmed using a β-galactosidase assay (A), which was induced using a galactose/raffinose carbon source. (B) Diluted cells were spotted onto auxotropic medium plates, namely leucine-depleted media. The interaction between Fpr in the bait vector and Fd in the trap vector was confirmed using a β-galactosidase assay. The average and standard deviation are shown in Fig. 4A.

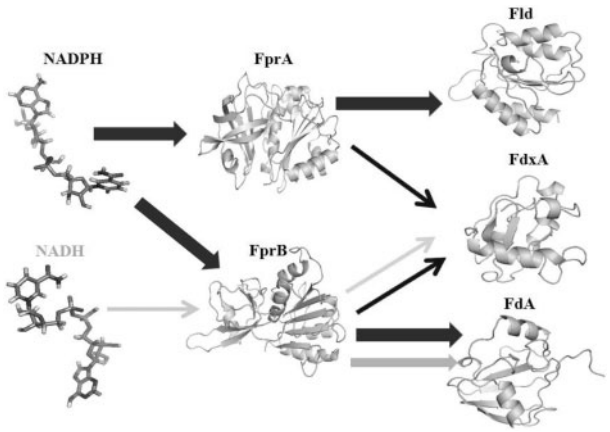

Fig. 5. **Proposed electron transfer by Fprs in *P. putida* KT2440.** The electron from electron flow from the NADH flow is represented by the grey colour, and the electron from flow from the NADPH flow is represented by the black colour. Values over 1.0 of k_{cat}/K_m are indicated by an arrow and the thickness of an arrow represent to catalytic efficiency (k_{cat}/K_m) of redox partner.

subclass Fprs in their chromosomes. However, function and electron partner of their Fprs are poorly understood. Here, we indentified the preferred physiological electron partners of both Fprs in *P. putida* for the first time. Based on the biochemical, physiological, genetic and structural data presented here, we propose expanding the traditional view of Fpr-related electron flow and functional plasticity of two Fprs in cell physiology (Fig. 5).

SUPPLEMENTARY DATA

Supplementary data are available at *JB* online.

FUNDING

This work was supported by a NCRC (National Core Research Center) grant (R15-2003-002-01002-0) and a Korea Science and Engineering Foundation (KOSEF) grant (R01-2008-000-10697-0) programs to W.P.

CONFLICT OF INTEREST

None declared.

REFERENCES

1. Carrillo, N. and Ceccarelli, E.A. (2003) Open questions in ferredoxin-NADP$^+$ reductase catalytic mechanism. *Eur. J. Biochem.* **270**, 1900–1915
2. Ceccarelli, E.A., Arakaki, A.K., Cortez, N., and Carrillo, N. (2004) Functional plasticity and catalytic efficiency in plant and bacterial ferredoxin-NADP(H) reductases. *Biochim. Biophys. Acta* **1698**, 155–165
3. George, D.G., Hunt, L.T., Yeh, L.S., and Baker, W.C. (1985) New perspectives on bacterial Ferredoxin evolution. *J. Mol. Evol.* **22**, 20–31
4. Ta, D.T. and Vickery, L.E. (1992) Cloning, sequencing, and overexpression of a [2Fe-2S] ferredoxin gene from *Escherichia coli*. *J. Biol. Chem.* **267**, 11120–11125
5. Birch, O.M., Hewitson, K.S., Fuhrmann, M., Burgdorf, K., Baldwin, J.E., Roach, P.L., and Shaw, N.M. (2000) MioC is an FMN-binding protein that is essential for *Escherichia coli* biotin synthase activity *in vitro*. *J. Biol. Chem.* **275**, 32277–32280
6. Green, J. and Paget, M.S. (2004) Bacterial redox sensors. *Nat. Rev. Microbiol.* **2**, 954–966
7. Imlay, J.A. (2006) Iron-sulphur clusters and the problem with oxygen. *Mol. Microbiol.* **59**, 1073–1082
8. Jung, Y.S., Gao-Sheridan, H.S., Christiansen, J., Dean, D.R., and Burgess, B.K. (1999) Purification and biophysical characterization of a new [2Fe-2S] Ferredoxin from *Azotobacter vinelandii*, aputative [Fe-S] cluster assembly/repair protein. *J. Biol. Chem.* **274**, 32402–32410
9. Jung, Y.S., Roberts, V.A., Stout, C.D., and Burgess, B.K. (1999) Complex formation between *Azotobacter vinelandii* ferredoxin I and its physiological electron donor NADPH-ferredoxin reductase. *J. Biol. Chem.* **274**, 2978–2987
10. Camba, R., Jung, Y.S., Hunsicker-Wang, L.M., Burgess, B.K., and Stout, C.D. (2003) Mechanisms of redox-coupled proton transfer in proteins: role of the proximal proline in reactions of the [3Fe-4S] cluster in *Azotobacter vinelandii* ferredoxin I. *Biochemistry* **42**, 10589–10599
11. Blaschkowski, H.P., Neuer, G., Ludwig-Festl, M., and Knappe, J. (1982) Route of flavodoxin and Ferredoxin reductase in *Escherichia coli*. CoA-acylating pyruvate: flavodoxin and NADPH: flavodoxin oxidoreductase participating in the activation of pyruvate formate-lyase. *Eur. J. Biochem.* **123**, 563–569
12. Sancho, J. (2006) Flavodoxins: sequence, folding, binding, function and beyond. *Cell. Mol. Life Sci.* **63**, 855–864
13. Tognetti, V.B., Zurbriggen, M.D., Morandi, E.N., Fillat, M.F., Valle, E.M., Hajirezaei, M.R., and Carrillo, N. (2007) Enhanced plant tolerance to iron starvation by functional substitution of chloroplast ferredoxin with a bacterial flavodoxin. *Proc. Natl Acad. Sci. USA* **104**, 11495–11500
14. Hu, Y., Li, Y., Zhang, X., Guo, X., Xia, B., and Jin, C. (2006) Solution structures and backbone dynamics of a flavodoxin MioC from *Escherichia coli* in both Apo- and Holo-forms: implications for cofactor binding and electron transfer. *J. Biol. Chem.* **281**, 35454–35466
15. Kurisu, G., Kusunoki, M., Katoh, E., Yamazaki, T., and Teshima, K. (2001) Structure of the electron transfer complex between ferredoxin and ferredoxin-NADP(+) reductase. *Nat. Struct. Biol.* **8**, 117–121
16. Sridhar-Prasad, G., Kresge, N., Muhlberg, A.B., Shaw, A., Jung, Y.S., and Burgess, B.K. (1998) The crystal structure of NADPH:ferredoxin reductase from *Azotobacter vinelandii*. *Protein Sci.* **7**, 2541–2549
17. Martinez-Julvez, M., Medina, M., and Gomez-Moreno, C. (1999) Ferredoxin-NADP(+) reductase uses the same site for the interaction with ferredoxin and flavodoxin. *J. Biol. Inorg. Chem.* **4**, 568–578
18. Lee, Y., Peña-Llopis, S., Kang, Y.S., Shin, H.D., Demple, B., Madsen, E.L., Jeon, C.O., and Park, W. (2006) Expression analysis of the *fpr* (ferredoxin-NADP+ reductase) gene in *Pseudomonas putida* KT2440. *Biochem. Biophys. Res. Commun.* **339**, 1246–1254
19. Lee, Y., Yeom, J., Kang, Y.S., Kim, J., Sung, J.S., Jeon, C.O., and Park, W. (2007) Molecular characterization of *fprB* (ferredoxin-NADP+ reductase) in *Pseudomonas putida* KT2440. *J. Microbiol. Biotechnol.* **17**, 1504–1512
20. Krapp, A.R., Rodriguez, R.E., Poli, H.O., Paladini, D.H., and Palatnik, J.F. (2002) The flavoenzyme ferredoxin (flavodoxin)-NADP(H) reductase modulates NADP(H) homeostasis during the soxRS response of *Escherichia coli*. *J. Bacteriol.* **184**, 1474–1480
21. Park, W., Pena-Llopis, S., Lee, Y., and Demple, B. (2006) Regulation of superoxide stress in *Pseudomonas putida* KT2440 is different from the SoxR paradigm in *Escherichia coli*. *Biochem. Biophys. Res. Commun.* **341**, 51–56
22. Pandini, V., Caprini, G., Thomsen, N., Aliverti, A., Seeber, F., and Zanetti, G. (2002) Ferredoxin-NADP+ reductase and ferredoxin of the protozoan parasite *Toxoplasma gondii* interact productively *in vitro* and *in vivo*. *J. Biol. Chem.* **277**, 48463–48471
23. Seo, D., Tomioka, A., Kusumoto, N., Kamo, M., and Enami, I. (2001) Purification of ferredoxins and their reaction with purified reaction center complex from the green sulfur bacterium *Chlorobium tepidum*. *Biochim. Biophys. Acta* **1503**, 377–384
24. Chapman, S.K. and Reid, G.A. (1999) *Methods in Molecular Biology*. Human Press, New Jersey, USA
25. Guex, N. and Peitsch, M.C. (1997) SWISS-MODEL and the Swiss-PdbViewer: an environment for comparative protein modeling. *Electrophoresis* **18**, 2714–2723
26. Thomsen-Zieger, N., Pandini, V., Caprini, G., Aliverti, A., and Cramer, J. (2004) A single *in vivo*-selected point mutation in the active center of *Toxoplasma gondii* ferredoxin-NADP$^+$ reductase leads to an inactive enzyme with greatly affinity for ferredoxin. *FEBS Lett.* **576**, 375–380
27. Comeau, S.R., Gatchell, D.W., Vajda, S., and Camacho, C.J. (2004) ClusPro: a fully automated algorithm for protein-protein docking. *Nucleic Acids Res.* **1**, W96–W99
28. Kozakov, D., Brenke, R., Comeau, S.R., and Vajda, S. (2006) PIPER: An FFT-based protein docking program with pairwise potentials. *Proteins* **65**, 392–406
29. Fischer, F., Raimondi, D., Aliverti, A., and Zanetti, G. (2002) *Mycobacterium tuberculosis* FprA, a novel bacterial NADPH-ferredoxin reductase. *Eur. J. Biochem.* **269**, 3005–3013
30. Wu, Y., Li, Q., and Chen, X.Z. (2007) Detecting protein-protein interactions by Far western blotting. *Nat. Protoc.* **2**, 3278–3284
31. Park, W., Jeon, C.O., and Madsen, E.L. (2002) Interaction of NahR, a LysR-type transcriptional regulator, with the alpha subunit of RNA polymerase in the naphthalene degrading bacterium, *Pseudomonas putida* NCIB 9816-4. *FEMS Microbiol. Lett.* **213**, 159–165
32. Hasan, M.N., Hagedoorn, P.L., and Hagen, W.R. (2002) *Pyrococcus* furiosus ferredoxin is a functional dimer. *FEBS Lett.* **531**, 335–338
33. Aliverti, A., Pandini, V., Pennati, A., de Rosa, M., and Zanetti, G. (2008) Structural and functional diversity of ferredoxin-NADP(+) reductases. *Arch. Biochem. Biophys.* **474**, 283–291
34. Bichet, A., Hannemann, F., Rekowski, M., and Bernhardt, R. (2007) A new application of the yeast

two-hybrid system in protein engineering. *Protein Eng. Des. Sel.* **20**, 117–123
35. Batie, C.J. and Kamin, H. (1986) Association of Ferredoxin-NADP$^+$ reductase with NADP(H) specificity and oxidation-reduction properties. *J. Biol. Chem.* **261**, 11214–11223
36. Giró, M., Carrillo, N., and Krapp, A.R. (2006) Glucose-6-phosphate dehydrogenase and ferredoxin-NADP(H) reductase contribute to damage repair during the *soxRS* response of *Escherichia coli*. *Microbiology* **152**, 1119–1128
37. Dos-Santos, P.C., Johnson, D.C., Ragle, B.E., Unciuleac, M.C., and Dean, D.R. (2007) Controlled expression of *nif* and *isc* iron-sulfur protein maturation components reveals target specificity and limited functional replacement between the two systems. *J. Bacteriol.* **189**, 2854–2862